Heliyon 10 (2024) e30447

Contents lists available at ScienceDirect

Heliyon

journal homepage: www.cell.com/heliyon

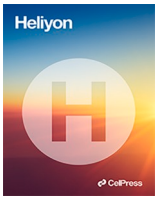

Research article

Laser-induced breakdown spectroscopy (LIBS) of animal fat (lard): Efficient sample preparation for onsite analysis and influence of sample temperature on the signal intensity and plasma parameters

M. Rashad Khan [b,c], R.K. Raja Ibrahim [a], M. Duralim [a], M.F. Omer [a], S.U. Haq [b,*]

[a] Department of Physics, Faculty of Science, Universiti Teknologi Malaysia, Johor Bahru 81310, Johor, Malaysia
[b] National Institute of Lasers and Optronics College, Pakistan Institute of Engineering and Applied Sciences, Nilore, Islamabad, 45650, Pakistan
[c] Department of Physics, University of the Poonch, Rawalakot, Azad Kashmir 12350, Pakistan

ARTICLE INFO

Keywords:
LIBS
Controlled sample temperature by thermoelectric cooling system
Lard
Signal enhancement
Sensitivity
Repeatability

ABSTRACT

We report an efficient sample preparation method (freezing) for onsite fat and meat analysis via a specially designed thermoelectric cooling and temperature-controlling system. This investigation also focused on the effect of phase change on the sensitivity and reproducibility of LIBS emission signals and plasma parameters. The plasma emissions of animal fats (lard) were recorded when the sample was frozen (−2 °C), fluid (15 °C), and in a liquid state (37 °C) with a thermoelectric cooling system. At each temperature, the plasma emissions were acquired at laser pulse energy from 50 to 300 mJ and detector gate delay (DGD) from 0.5 to 5 μs. With increasing sample temperature, the DGD, where the optical emission intensity reached a maximum, decreased. At a laser pulse energy of 200 mJ and a sample temperature of −2 °C, the emission signals increased fourfold, the signal-to-noise ratio (SNR) improved tenfold, and the self-absorption in the emission lines decreased significantly. The repeatability of the emission signals and plasma parameters of frozen and liquid fat samples was determined using the relative standard deviation (RSD) of Se I (473.08 nm) and K I (766.48 nm) emission lines. The RSDs of the emission signals improved from 40 to 18 % and 37 to 16 %, whereas the shot-to-shot RSDs of the electron temperature and electron number density get improved from 11 to 6 % and 12 to 6.8 %, respectively.

1. Introduction

This work is part of the project to design and develop an automated and autofocus LIBS system to discriminate and compositionally analyze different meat and fat products. To develop such a system, laboratory work included sample preparation and cooling as well as temperature control for onsite analysis on the market. Various parameters, such as sample temperature, laser energy, DGD, and lens-to-sample distance, were studied and optimized in this work. These parameters need to be optimized to get enhanced emission, better SNR, and repeatability of LIBS emission signals and plasma parameters. These optimized experimental parameters will be used in the final LIBS system because the meat and fats on the market are usually frozen but may exist in a semiliquid form at room temperature. Lard is a semisolid, soft, and butter-like fat obtained by heating or boiling the fatty tissues of hogs. The saturated fats in animal meat, cheese, butter, milk, and cream are waxy at room temperature. It is used in foods for its flavor [1], is mixed in oils [2–4], and is used in

* Corresponding author.
E-mail address: sami_ulhaq2002@yahoo.com (S.U. Haq).

https://doi.org/10.1016/j.heliyon.2024.e30447
Received 7 November 2023; Received in revised form 25 April 2024; Accepted 26 April 2024
Available online 27 April 2024

making soap, candles, and biodiesel [5]. LIBS is a powerful analytical technique that is widely used for the compositional analysis of a variety of materials, including foods. Food colors are analyzed to detect heavy metals, which may cause adverse health effects [6]. Similarly, LIBS has been used for the in situ detection and identification of natural and added fake elements in saffron, radish, and cornsilk [7]. The Pb contents of tea samples collected during the three seasons were analyzed. The detection limit of Pb in these samples was determined to be 48.4 mg kg^{-1} [8]. A review on laser-induced breakdown spectroscopy (LIBS) of food analysis by Maria et al. [9] comprehensively reviewed the progress and applications of LIBS for assessing the composition and quality of food products such as meat, bakery items, vegetable oils, cereals, etc.

In the LIBS technique, an intense laser beam is used to produce plasma on the sample surface, which produces characteristic spectral signatures that can be utilized to identify and quantify the sample constituents [10,11]. LIBS can provide fast and nondestructive analysis of samples, making it an attractive method for food industry applications. Additionally, LIBS has the potential to detect contaminants and adulterants in foods, making it an essential tool for food safety and quality control. Overall, LIBS is a promising technique for analyzing samples in any state (solid, liquid, and gas), offering a quick, accurate, and non-destructive way to determine the composition and quality of the sample under study. These features of LIBS make it advantageous over existing analytical techniques [12]. Despite these advantages, LIBS also has some challenges and limitations that can pose problems in specific applications. These include the matrix effect, low sensitivity, signature interference, and poor repeatability. These problems arise from the chemical and physical properties, morphology, and composition of the sample and become worse for creamy and waxy samples than for solids due to cavitation, splashing, a shorter plasma duration, and coating optics [13]. As a result laser matter interaction is significantly affected which results less sensitive and least repeatable analytical results. To overcome the high signal variability and low sensitivity associated with LIBS of creamy or waxy targets such as fat, a strategy is essentialy required. However, some techniques, such as laminar flow [14,15], liquid-to-aerosol conversion [16,17], and microdroplet approaches [18–21], have been adopted to achieve better sensitivity by avoiding splashing, bubbles, and cavitation in LIBS analysis of liquids. However, these strategies are only suitable for some creamy and waxy samples.

Liquid-to-solid conversion by freezing is another strategy to avoid splashing, bubbles, cavitation, and material clogging. Once these issues are eliminated, the LIBS signal sensitivity and repeatability improve enough and can be applied to analyze creamy and waxy samples. To date, few researchers have used this technique only for LIBS analysis of liquid samples. Sobral et al. [22] compared the limits of detection (LODs) of trace elements in solidified samples (ice) with those in liquid nitrogen and water. The results show that the average LOD of the traces in the solidified sample was six times greater than that in water under the same experimental conditions. Similarly, Borges et al. [23] used calibration-free LIBS (CF-LIBS) for the compositional analysis of aqueous solutions (Mg $(NO_3)_2$, Zn $(NO_3)_2$, NaCl and KCl in distilled water) frozen by immersion in liquid nitrogen. However, liquid-to-solid conversion with the liquid nitrogen technique still faces problems of temperature control and sample contamination. Another membrane-based liquid-to-solid conversion method was used to solidify the aqueous metal solutions, which enhanced the quantitative analysis and decreased the LOD up to μg/kg but could not improve the accuracy as compared to existing analytical techniques, such as inductively coupled plasma optical emission spectroscopy (ICP–OES) [24]. Syaida Hanasil et al. [25] froze the extracted fats of chicken, lamb, beef, and lard with liquid nitrogen and a freezer and recorded their emission spectra. They observed that frozen chicken and lamb samples showed stronger emission signals when solidified with liquid nitrogen, whereas beef fat and lard emission signals substantially increased when solidified in the freezer.

The above cited literature indicates that the analysis of fats at room temperature suffers from low sensitivity and low LOD. Alternatively, solidification by a thermoelectric temperature controlling system, the one used in the present work, enabled us to convert liquid into solid by freezing without contamination and facilitated to maintain temperature of a sample to study the effects of sample temperature and viscosity on the LIBS spectra. Therefore, the objectives of the present work were to investigate the impact of the sample phase on the emission signal intensities and plasma parameters by controlling the sample temperature and optimizing other experimental parameters, such as the laser energy and DGD. Furthermore, this work also aimed to find an optimized set of experimental parameters for better signal enhancement, improved SNR, and increased repeatability of plasma parameters. To achieve these improvements, a thermoelectric cooling and heating system is designed and installed to freeze and control the temperature of fat. Under these arrangements, the plasma was produced on the surface of the fat sample as a function of temperature, laser ablation energy, and DGD to get optimized experimental conditions for signal enhancement, SNR, and repeatability in emission signals and plasma parameters. In addition, the separation between lens and sample, and position of the optical fiber for light collection were optimized.

The novelty of this work mainly comes from the use of thermoelectric cooling and a sample temperature controlling system, which freezes the sample on the spot, enabling us to freeze and analyze the sample on site (in the meat market). Furthermore, due to ablation, the sample temperature may increase and melt the top layer of fat, which increases the shot to shot variation in emission signals, and the melting of the top layer may produce problems associated with the LIBS of the molten sample. The sample, frozen using a freezer or liquid nitrogen, cannot be applied on-site for online analysis, and the sample may melt after ablation. It is well known that the LIBS spectral signal of frozen fat is stronger, but in this work, we report that the repeatability also increased twofold.

2. Experimentation

2.1. Sample

In this study, we have used lard samples, which are extracted by the procedure as described in our work [25] to perform its LIBS as a function of DGD and laser energy in its frozen, molten or liquid (melted) state. Fresh pork meat was collected from Taman University's

market near Johor Bahru, Malaysia, to extract the fat. It was rinsed with plenty of water, dried and cut into small pieces, placed into an oven for melting, and finally poured into the jar. Fig. 1(a–e) shows the sample preparation steps.

We put 1 mL of extracted animal fat (lard) in a small dish and placed it on the sample stage, which we fitted with a thermoelectric system. The temperature of the thermoelectric system was set as required and kept the sample for a while to become stable. A thermal sensor was placed close enough to record the sample's temperature accurately. This thermoelectric system allows us to solidify liquid samples within 5 min. Therefore, solidifying liquid samples with a thermoelectric system is better than other solidification methods, such as liquid nitrogen or a freezer.

2.2. Thermoelectric cooling and heating setup

A thermoelectric cooling and heating setup was used to freeze the sample and maintain its temperature during the experiment. This system consists of a thermoelectric module and a temperature-controlling unit as shown in Fig. 2 (a,b). The thermoelectric module, represented in Fig. 2(a), comprises a Peltier, heat sink, cooling fan, and water-circulating unit, whereas the temperature-controlling unit includes a heat sensor and temperature display unit, as depicted in Fig. 2(b).

2.3. Experimental setup

The schematics of the experimental setup to produce a laser-induced plasma of lard and to record the plasma emissions are shown in Fig. 3. The Q-switched Nd: YAG (Quantel Q-Smart-850) laser operating at 1064 nm, with the 10 Hz repetition rate and pulse width of 5–6 *n*s was employed as an ablation source. The laser pulse was focused orthogonally on the surface of the sample with a lens having a focal length of 5 cm, which produced a spot size of ~200 μm on the sample. As a result, plasma of lard was produced, and the plasma light was transmitted to the compact CCD spectrometer (Thorlabs CCS 200, Germany) through a multimode quartz optical fiber having a core diameter of 200 μm. One end of the optical fiber has a collimating lens positioned at 45° with reference to sample surface and 3 mm away from the breakdown location. The collimating lens has a 5 mm focal length. It collects the optical emissions and transfers them to the entrance slit of a spectrometer. The spectrometer covers the wavelength range of 200–1000 nm with variable integration time and spectral resolution is < 0.2 nm. The spectrometer dispersed the plasma light at different angles and recorded as a spectrum. The laser system and the LIBS spectrometer were synchronized through a delay generator (DG 535, Stanford Research System, Inc. USA).

The sample temperature (T) was controlled by a thermoelectric module, which consists of a Peltier (TEC1 12,706, Quick-cool, Germany), thermal sensor and controller. The working range of this module is from −5 °C to 40 °C (±0.1 °C) and was attached to a 2D movable stage. The digital thermometer and the temperature-controlling sensor are factory-calibrated with ±0.1 °C accuracy. In these experiments, the extracted fat (lard) was placed on the moving platform, which made available a new location for each laser shot. The separation between lens and sample was fixed in a way to minimize the breakdown of ambient air just above the surface of the sample. Prior to ablation, the temperature of the thermoelectric system was fixed at a particular value and let the sample stabilize. Thereafter, laser was fired and plasma was produced at 50–300 mJ per pulse, at sample temperatures (−2, 15, and 37 °C) and recorded with DGD (0.5–5 μs). Multiple emission lines of the sample's constituents were qualitatively analyzed with the help of NIST atomic database [26], MATLAB code, and the electric dipole and intensity selection rules. MATLAB code utilizes the spectral position of emission lines to match them with the transitions given in the NIST database. The analyzed emission spectra were used to investigate the self-absorption, sensitivity, and reparability in line intensities, electron temperature, electron number density and analytical results.

3. Results and discussions

3.1. Emission spectra of animal fat lard

The plasmas of the lard (fat) sample were produced at 200 mJ laser pulse energy, at −2 °C, 15 °C, and 37 °C sample temperatures, and at 2, 1.5, and 1 μs DGD. The values of DGD were selected for each sample temperature where the maximum signal intensities were

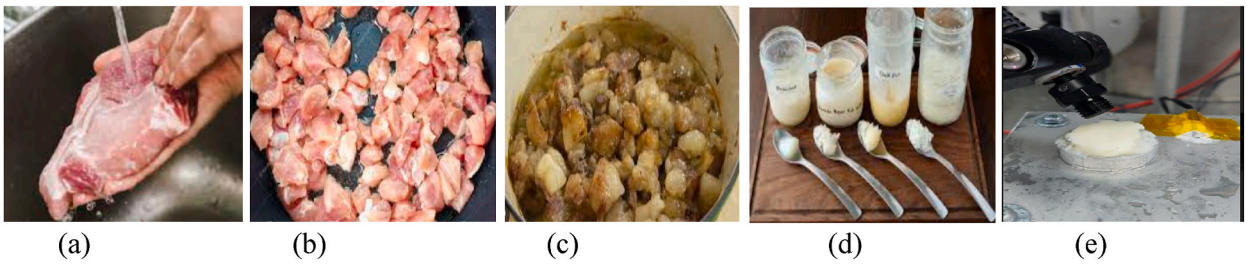

Fig. 1. (a–e): Sample preparation steps, including: (a) rinse with water, (b) cut into small pieces, (c) melting in oven, (d) putting in jar, (e) prepared sample for LIBS experiments.

(a) Thermoelectric module (b) Temperature controlling

Fig. 2(a. b): Peltier based thermoelectric cooling and temperature-controlling unit with thermal sensor.

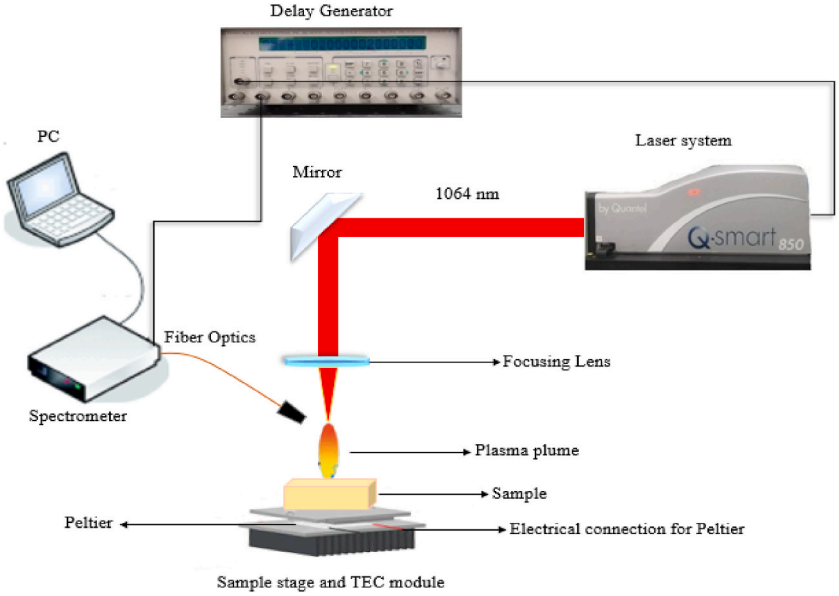

Fig. 3. Schematics of LIBS experimental setup.

obtained. The emission spectra of laser-induced plasmas at these experimental parameters were recorded. At a sample temperature of 37 °C, an enhanced signal intensity was obtained at a DGD of 1 μs, whereas at a sample temperature of −2 °C, the best emission signal intensity was obtained at a DGD of 2 μs. Fig. 4 (a, b) illustrates the recorded emission spectra in the 400–800 nm spectral range, showing the selected emission lines. In this figure, the upper trace (Fig. 4(a)) is recorded at T = 37 °C (DGD = 1 μs), while the lower trace (Fig. 4(b)) is recorded at T = −2 °C (DGD = 2 μs). It is observed that signal intensity significantly enhanced when the sample was frozen. As shown in Fig. 4 (b), some new emission lines also appeared, proving that the sensitivity increased when the sample was frozen. It is also observed that the enhancement in signal intensity is element dependent because it depends on the spectroscopic parameters of the emitted line of an element.

3.2. Dependence of signal intensities of trace elements on the sample temperature, laser energy, and DGD

Fig. 5(a–c) shows the variation in the signal intensities of essential trace elements such as selenium (Se), zinc (Zn), and potassium (K) in the extracted fat (lard) with respect to the laser energy and detector delay at a fixed temperature (T = −2 °C). The signal intensities used were background subtracted. To get optimized experimental parameters, the laser energy was varied from 50 to 300 mJ, and the DGD was varied from 0.5 to 5 μs at fixed sample temperatures of −2, 15, and 37 °C. The signal intensities of the trace elements almost linearly increase with increasing laser pulse energy from 50 to 200 mJ, but thereafter, a slow decreasing trend is observed up to 300 mJ. This is because of more material ablation with increasing laser energy, which results in more hot plasma, but at higher ablation energies, the emission line intensities get saturated, as illustrated in Fig. 5(a–c). These figures also show the variation in signal intensities with DGD, which measures the laser-induced plasma lifetime. To study the influence of plasma lifetime, the DGD was varied from 0.5 to 5 μs for each laser energy at a fixed sample temperature. The emission line intensities are initially small, increase with

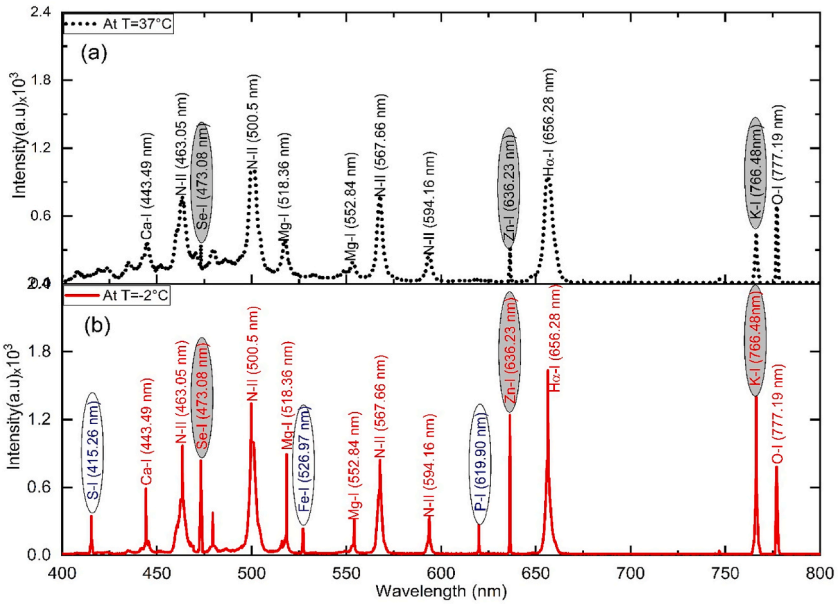

Fig. 4. (a, b): The emission spectra of lard produced at 200 mJ pulse energy and at sample temperatures and recorded at DGD of (a) 37 °C, 2 μs and (b) −2 °C, 1 μs?

delay, and reach a maximum at a 2 μs delay. After that, it again decreased smoothly up to 5 μs for all values of laser energy. Moreover, it is also observed that the variation in signal intensity is different for different elements because the emission line intensities depend on the spectroscopic parameters of the emitted line of an element. Background continuum emission due to free-free transitions (Bremsstrahlung) and free-bound transitions is dominant in the early stage of the plasma, and its rate of decay is faster than that of atomic emissions. Therefore, an optimum signal could be recorded with a sDGD. Fig. 5(b) shows that the maximum signal intensity is achieved at a laser energy of 200 mJ and a DGD of 2 μs, which are the optimized values for a sample temperature of −2 °C.

The line emission intensity increased linearly with increasing laser energy due to an increase in the amount of ablated material. However, at much higher energies (>200 mJ), saturation of the line intensities appeared because of self-absorption in the emission lines due to plasma shielding. The self-absorption distorts the spectral line profile, resulting in a flat top and broadened the line profile. The self-absorption is element dependent as well as depends on the line emission characteristics, elemental concentration, and laser ablation energy. Saturation in emission line intensities, along with its underlying reasons, was reported by Russo [27].

Additionally, the recorded signal intensities were well below the saturation threshold of the CCD detector of the spectrometer. Fig. 6illustrates the least or no self-absorbed emission line (N II (567.95 nm) and highly self-absorbed emission lines, recorded at 150 mJ, 200 mJ, and 250 mJ Laser energies, respectively. This kind of self-absorption as a function of laser energy is also reported by Chen et al. [28].

Furthermore, to investigate the effect of the sample's temperature on emission signal intensities and lifetime of laser-induced fat plasma, the SNRs of Se, Zn, and K were plotted as a function of DGD at different sample temperatures because the plasma lifetime of liquids or organic samples significantly depends on the physical state of the sample. This is a more focused aspect of the current study. Fig. 7(a–c) illustrates the variation in the SNR as a function of DGD at −2 °C (frozen form), 15 °C (melted state), and 37 °C (liquid state) at a fixed optimized laser energy of 200 mJ. These figures show that the SNR varies similarly for all three elements. Moreover, the DGD becomes increasingly shorter for the maximum signal intensity with increasing sample temperature. This is because when the sample was at −2 °C (frozen sample), the laser-matter interaction was efficient, and more mass ablated, making the laser-induced plasma more intense and long-lasting. However, with increasing sample temperature, melting starts, and mechanical effects, like splashing, ripples on the surface, and shockwave deteriorate the laser matter and laser plasma interaction. Consequently, short-lived and weakly ionized plasmas are produced. From the above discussion, it is clear that laser energy = 200 mJ, T = −2 °C, and DGD = 2 μs are the optimized experimental parameters where maximum signal enhancement was achieved. Compared to those of molten samples, efficient laser ablation, signal enhancement, and improved repeatability of results are well documented in the literature. When a laser pulse vaporizes the molten sample, miniature shock waves create particles above the sample surface, disrupting the incident laser pulse, and a smaller amount of plasma light reaches the spectrometer. Moreover, the shock waves induced on the surface of the liquid increase the pulse-to-pulse variation in emission signal, and consequently, the RSD increases. The interaction of a laser with a molten sample also generates bubbles inside the liquid that are transparent to the laser beam. These bubbles could come up the surface of the liquid and affect the characteristics of the plasma, consequently reducing the signal repeatability. . The angle of incidence of laser changes, which varies the laser fluence and signal intensities of the emitted light [29,30].

The sensitivity of LIBS can be quantified by measuring the SNR, which utilizes the line intensity and the standard deviation of background, in the following expression;

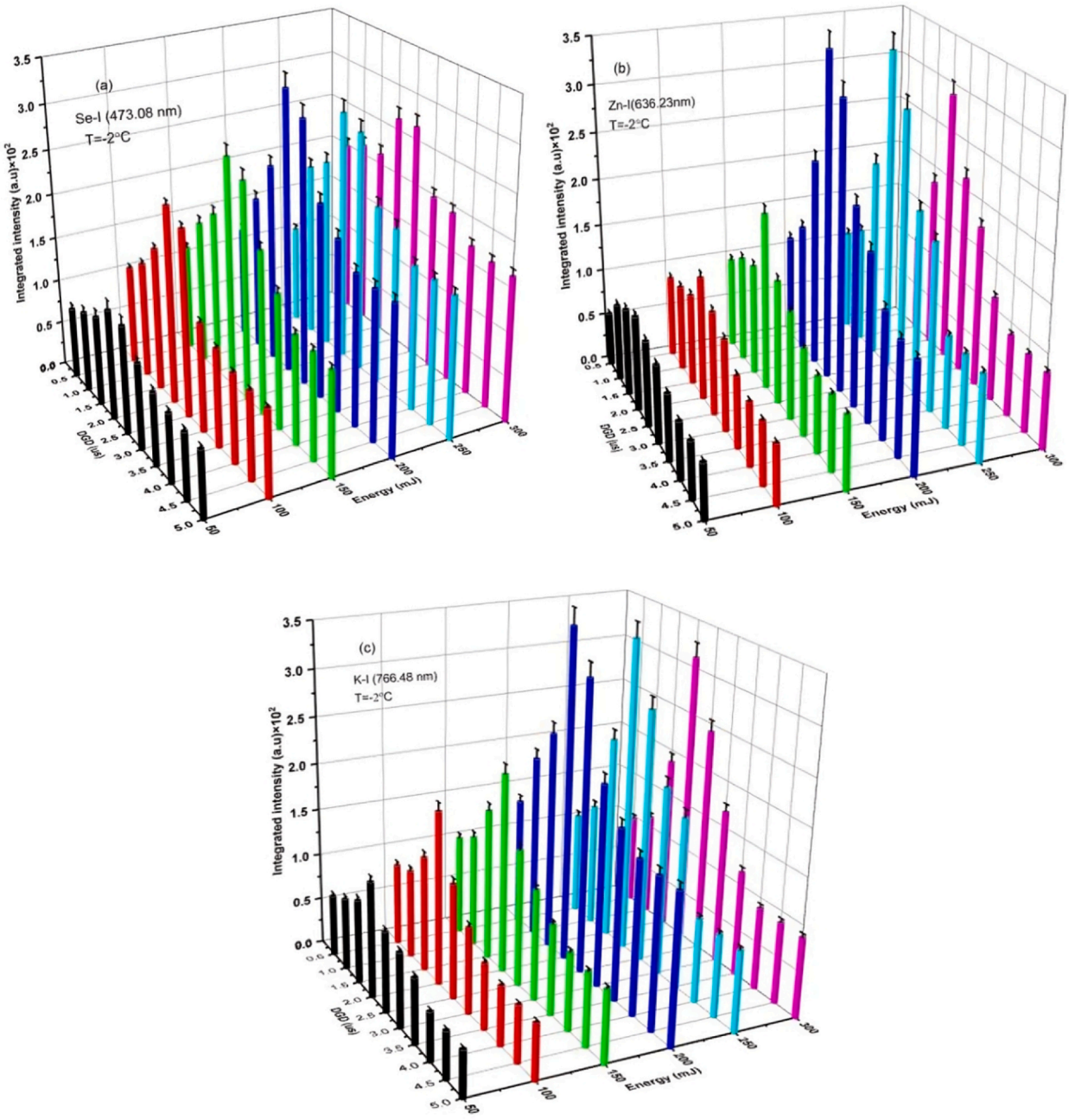

Fig. 5(a–c). Variation in emission line intensities of (a) Se I (473.08 nm), (b) Zn I (636.23 nm), and (c) K I (766.48 nm) with laser energy and DGD at a sample temperature T = −2 °C.

$$\mathrm{SNR} = \frac{I}{\sigma_b} \tag{1}$$

Where I is the integrated spectral line intensity and σ_b is the background standard deviation.

In the present study, spectral lines of essential trace elements such as Se I (473.08 nm), Zn I (636.23 nm), and K I (766.48 nm) were used to measure the SNR at two extreme sample temperatures (−2, °C, 37 °C) and at an optimized set of experimental parameters (laser energy of 200 mJ and DGDs of 2 μs and 1 μs). Fig. 8 shows that at −2 °C, the SNRs of Se, Zn, and K increased by factors of 20, 3, and 2.5, respectively. The enhancement in the SNR may be due to efficient laser-matter interactions, the minimization of splashing, cavitation, and shockwave generation. In this study, the emission signals were significantly enhanced when the sample was solidified, and its temperature was controlled with a thermoelectric system. With this enhancement, the SNR ratio and LOD improved, but the LOD could

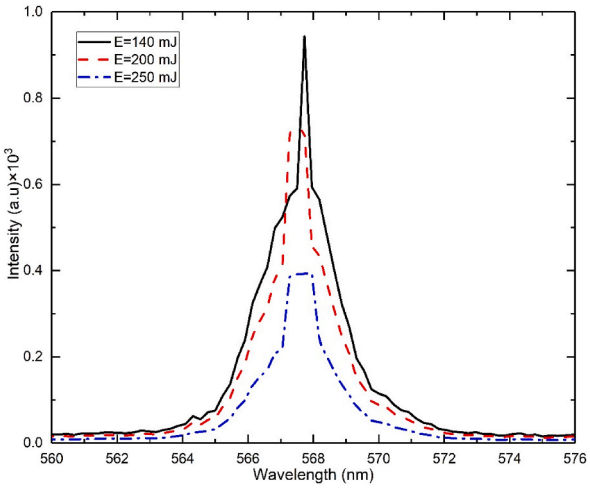

Fig. 6. Line profile of N-II (567.95 nm) emission line, as a function of laser energy, showing high degree self-absorption when spectra recorded at 200 mJ and 250 mJ.

not be quantified due to the unavailability of reference samples. However, from the existing data, we determined that the standard deviations of the background at −2 and 37 °C are 0.0041 and 0.056 for Se I (473.08 nm), 0.00015 and 0.063 for Zn I (636.13 nm), and 0.00052 and 0.0061 for K I (766.48 nm). These calculations show that the detection limit improved due to a significant decrease in the standard deviation as one factor. The other factor, the slope of the calibration curve, could not be determined for the reasons mentioned above.

3.3. Shot-to-shot repeatability in signal intensities and plasma parameters

The repeatability of experimental results is always required for accuracy and reliability. Therefore, this section investigates the shot-to-shot repeatability of emission signals and plasma parameters at a particular set of experimental parameters, using frozen samples. The experimental parameters including laser pulse energy, DGD, position of the collimator for light collection, and lens to sample distance, were optimized as recommended in Ref. [31]. With these optimized experimental settings, the emission spectra of fat were recorded at sample temperatures of −2 °C, 15 °C, and 37 °C, and the DGDs were 2 μs, 1.5 μs, and 1 μs, respectively. The variations in the RSDs of the integrated intensities of Se I (473.08 nm) and K I (766.48 nm) as a function of laser energy at the extreme sample temperatures and corresponding DGDs are shown in Fig. 9 (a). It is evident from the figure that although the variations in the RSDs of the emission signals with respect to the laser ablation energy are similar for sample temperatures of −2 °C and 37 °C, the signal fluctuations (RSD) are significantly reduced at −2 °C. With increasing laser energy up to 150 mJ, the RSD swiftly decreased, but thereafter, it slowly increased up to 300 mJ. At 150 mJ, the signal repeatability of the frozen sample was approximately 50 % greater than at 37 °C of sample temperature. This is due to efficient laser-matter interactions when the sample is frozen, resulting in a long-lived plasma with low signal-to-noise fluctuations. Thus, at a laser energy of 150 mJ, the precision is at its highest but again depends on the sample temperature and nature of the emitted line. Furthermore, the RSDs of the integrated intensities of the two emission lines as a function of sample temperature are plotted in Fig. 9 (b). The increasing trend in RSDs shows that emission signal intensities are more repeatable as long as the sample remains frozen, but after 10 °C, the RSDs increase almost linearly with sample temperature. The increase in the signal fluctuations of fat with increasing sample temperature is due to the splashing of the material on the optics, bubble cavitation, decreasing plasma lifetime, and shockwaves when sample starts melting. With increasing sample temperature, these mechanical effects become increasingly stronger as the sample melts, and the radiative energy from laser-induced plasma fluctuates.

Hence, it is concluded that the repeatability is sufficiently improved at a sample temperature of T = −2 °C. To check the measurement-to-measurement repeatability of the emission signals, two emission lines of trace elements, Se I (473.08 nm) and K I (766.48 nm), were selected from the fat spectra and recorded at a laser energy of 150 mJ, sample temperatures of −2 °C, 37 °C and corresponding DGDs (2 μs, 1 μs). Fig. 10 (a, b) represents the average integrated intensity of six laser shots and forty such data points with average RSD. The measurement-to-measurement fluctuation in the integrated intensity may be due to the physical state of the sample, laser energy fluctuations, sample inhomogeneity, and variation in surface texture. At a sample temperature of 37 °C, the shot-to-shot stability of the emission signal is very poor, significantly improving at a sample temperature of −2 °C. These reduced signal fluctuations may be attributed to sample freezing and controlling the sample temperature to ±0.1 °C for all laser shots. However, there is room for further improvement in accuracy and repeatability. Fig. 10 (a, b) shows that the RSDs of Se I (473.08 nm) and K I (766.48 nm) improved from 40 % to 18 % and from 37 % to 16.2 %, respectively, when the sample temperature decreased from 37 °C to −2 °C.

Furthermore, the repeatability in electron temperature and electron number density was evaluated at sample temperatures of −2 °C and 37 °C under optimized experimental parameters (laser energy = 150 mJ, DGD = 2 μs for −2 °C and 1 μs for 37 °C). The

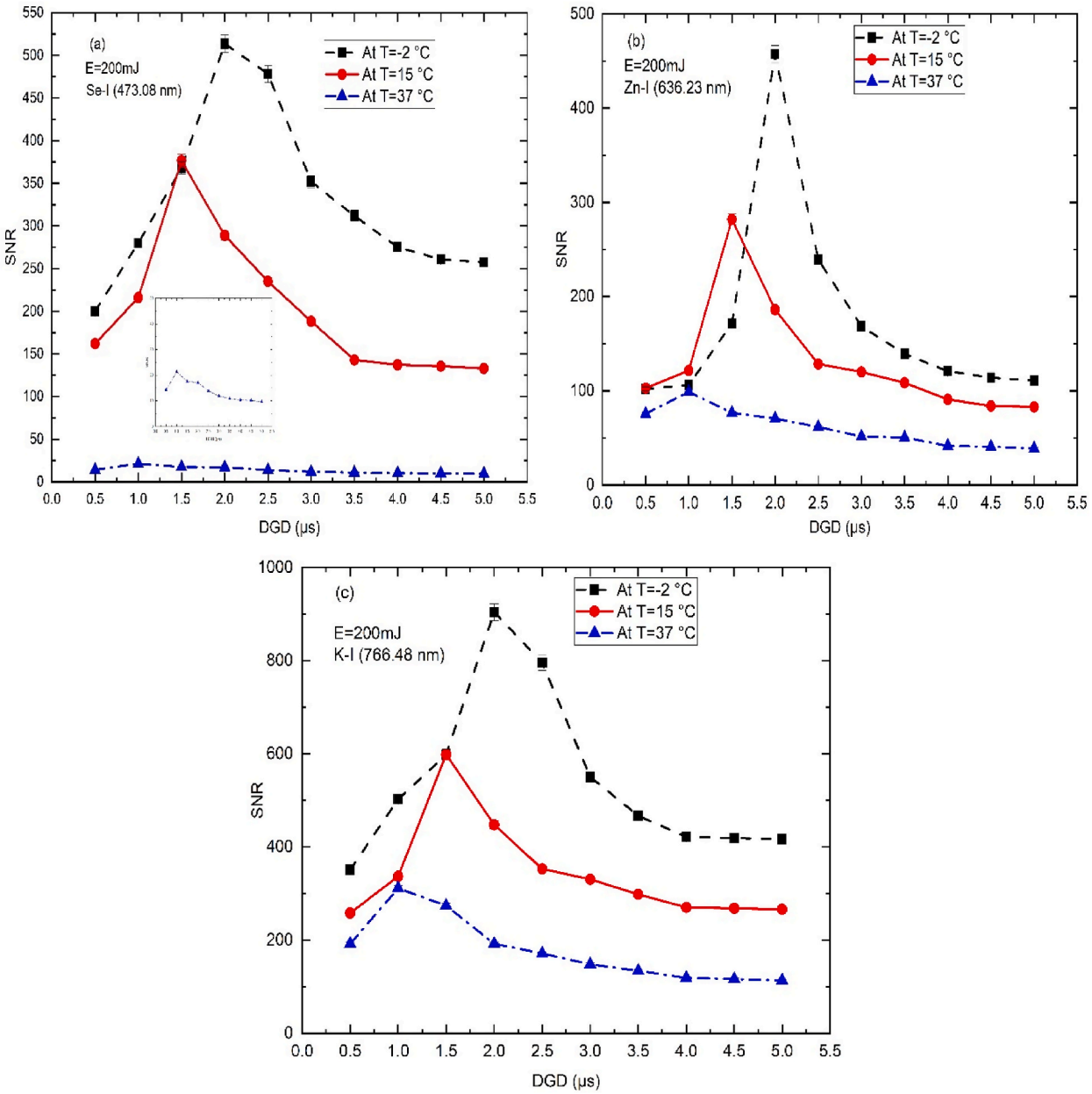

Fig. 7. (a–c): Variation in SNR of trace elements (a) Se I (473.08 nm), (b) Zn I (636.23 nm), and (c) K I (766.48 nm) of lard (fat) relative to DGD at 200 mJ laser energy and sample temperatures (T) of −2 °C, 15 °C, and 37 °C.

temperature of the lard plasma was determined using the intensity ratio and Boltzmann plot methods [32–34]. Table 1 shows that the Mg I emission lines were employed in the intensity ratio formula (Eq. 2), which yielded plasma temperatures of 9000 K and 8000 K.

$$\frac{I_I}{I_{II}} = \frac{\lambda_{II}}{\lambda_I}\frac{A_{kI}}{A_{kII}}\frac{g_I}{g_{II}}\exp\left[\frac{-(E_I - E_{II})}{K_B T_e}\right] \tag{2}$$

where I_I, I_{II}, E_I, and E_{II}, $A_{KI}, A_{KII}, g_I, g_{II}$ are the integrated intensities, upper-level energies, transition probabilities, and statistical weights of lines I and II, respectively, and K_B is the Boltzmann constant and T_e plasma temperature.

The self-absorption in emission lines, used for the determination of plasma parameters, was evaluated and corrected with the internal reference self-absorption correction (IRSAC) approach. The plasma temperature was extracted from the following Boltzmann plot method, which utilized the emission lines of N II, as listed in Table 2.

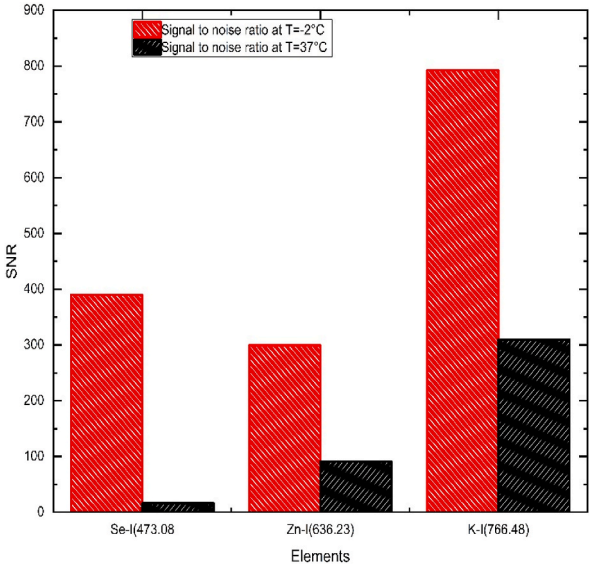

Fig. 8. SNR of trace elements (Se I (473.08 nm), Zn I (636.23 nm), and K I (766.48 nm) at 200 mJ laser energy and DGDs of 2 μs, 1 μs?

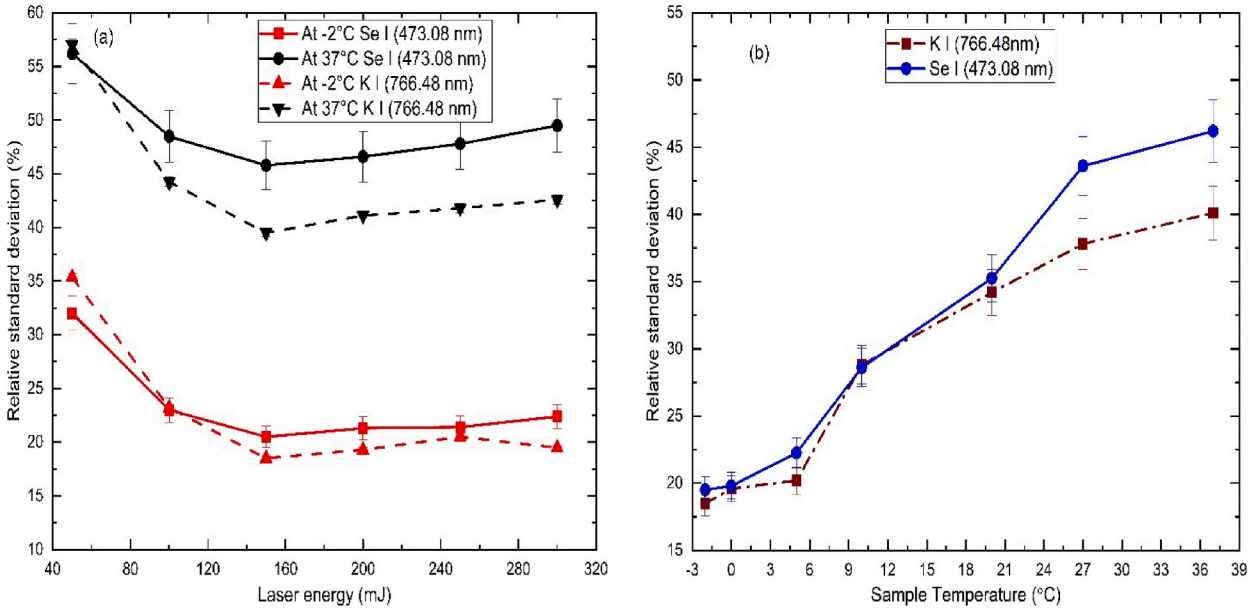

Fig. 9. (a, b): RSD of the emission lines of Se–I (473.08 nm) and K–I (766.48 nm) as a function of laser energy and (b) sample temperatures at E = 150 mJ. The experimental parameters were DGD 2 μs, 1 μs, and sample temperatures (T) −2 °C and 37 °C, respectively.

$$\ln\left(\frac{\lambda \mathrm{I}}{A_j g_j}\right) = -E_j/k_B T_e + In\left(\frac{FC_s}{\mathrm{U}(T_e)}\right) \tag{3}$$

Where λI is the product of the integrated intensity and wavelength of a line and A_j, g_j, and Ej are the transition probability, statistical weight, and upper state energy, respectively. Factor F is the optical collection system efficiency, C_s is the species concentration, $U(Te)$ is the partition function, and T_e is the plasma temperature. Each set of data points (ln *term of* E_j) represents a point on the Boltzmann plot, and the linear fit of such data points yields the slope ($m = -\frac{1}{K_B T_e}$), which yields plasma temperatures of 8900 K and 7500 K. Both plasma temperatures are obtained. The uncertainty in the plasma temperature is 10 % due to the uncertainties in the emission line intensities, transition probabilities, and fitting methods. In either approach, the higher electron temperature for the frozen state (−2 °C) of the sample is due to better laser-matter interactions and the minimization of splashing, bubble cavitation, and ripples.

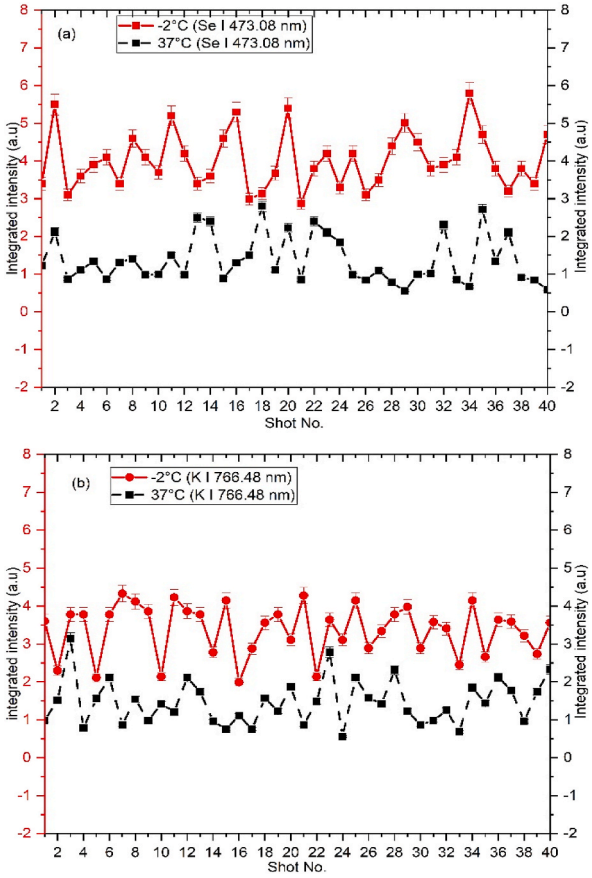

Fig. 10. (a, b): Pulse to pulse variation in emission line intensities and the resultant RSD for Se I (473.08 nm) and K I (766.48 nm) at sample temperatures of -2 °C (red) and 37 °C (black). The data was acquired at laser energy 150 mJ and DGD 2 μs (T = −2 °C), and 1 μs (T = 37 °C). (For interpretation of the references to color in this figure legend, the reader is referred to the Web version of this article.)

Table 1
Parameters of two neutral magnesium lines for plasma determination.

Wavelength (λ) nm	Upper-level Energy (E_k) eV	Transition probability (A_k) $\times 10^7 s^{-1}$	Statistical weight (g_K)
Mg I (518.36)	5.11	6.62	3
Mg I (552.84)	6.58	1.40	3

Table 2
Spectroscopic data of nitrogen emission lines were used to determine electron temperature using the Boltzmann plot method.

Wavelength (λ) nm	Upper-level Energy (E_k) eV	Transition probability (A_k) $\times 10^7 s^{-1}$	Statistical weight (g_k)
N II (463.05)	21.16	7.48	5
N II (500.52)	23.14	11.4	9
N II (567.60)	20.65	2.8	3
N II (594.16)	23.25	5.47	7

The electron number density (N_e) was determined using the Stark broadened emission line of Mg I (552.84 nm) in the following expression [35].

$$N_e\left(cm^{-3}\right) = \left(\frac{\Delta\lambda_{1/2}}{2w}\right) \times 10^{16} \tag{4}$$

Where $\Delta\lambda_{1/2}$ is the full-width at half-maximum (FWHM) and w is the electron impact broadening parameter. The value of w for the Mg I (552.84 nm) line is 0.24 A^0 [36], whereas $\Delta\lambda_{1/2}$ was extracted using Lorentzian fitting over the Mg line profile. Using these parameters in Eq. (4), the electron number densities are extracted as $1.55 \times 10^{17}/cm^3$ and $0.9 \times 10^{17}/cm^3$ at sample temperatures of −2 °C and

37 °C, respectively. The higher density for the sample at a temperature of −2 °C was due to the efficient laser-matter interaction when the sample was frozen. Thus, more material ablates, producing long-lived and efficient plasma.

Fig. 11 (a) shows that the measurement-to-measurement variation in plasma temperature for the frozen sample (at −2 °C) is less than that indicated by the 6.5 % RSD compared to the sample temperature of 37 °C, where RSD = 11 %. Similarly, Fig. 11 (b) shows a lower shot-to-shot variation in N_e with RSD (6.8 %) for the frozen sample than for the sample at 37 °C. In case of frozen fat, the higher repeatability (lower RSD) of the plasma parameters is due to the reduced mechanical effects as compared to the sample at room temperature.

4. Conclusion

The effects of sample temperature, laser energy, and DGD on the sensitivity and repeatability of LIBS of extracted fat (lard) were studied using a LIBS setup fitted with a thermoelectric cooling and heating system. Compared to existing sample freezing techniques such as liquid nitrogen and placing the sample in a freezer, the one used in this work is straightforward, and the sample temperature can be controlled to the desired value. When the sample temperature (T) was increased from −2 °C to 37 °C, the maximum signal enhancement was achieved at a shorter DGD. Thus, the optimized DGD and laser energy values for the maximum signal intensity and improved SNRs were 2 μs (for −2 °C), 1 μs (for 37 °C), and 200 mJ. Approximately four times greater signal enhancement and ten times greater SNR were obtained at a sample temperature of −2 °C than at 37 °C. Improved repeatability, as indicated by low RSDs in the emission signal and plasma parameters, was achieved for frozen sample as compared to when the sample was at 37 °C. The work on signal enhancement, sensitivity, and repeatability will be extended further to DP-LIBS of liquid samples under controlled sample temperatures and gaseous environments.

Funding

This work is financially supported by the Ministry of Education Malaysia under the fundamental research grant scheme vot no. 5F551.

Data availability statement

All the data used in this work is contained in this article, and therefore, no data is deposited separately into a publicly available repository.

CRediT authorship contribution statement

M. Rashad Khan: Writing – original draft. **R.K. Raja Ibrahim:** Supervision, Conceptualization. **M. Duralim:** Formal analysis. **M.F. Omer:** Writing – review & editing. **S.U. Haq:** Writing – review & editing, Supervision, Methodology.

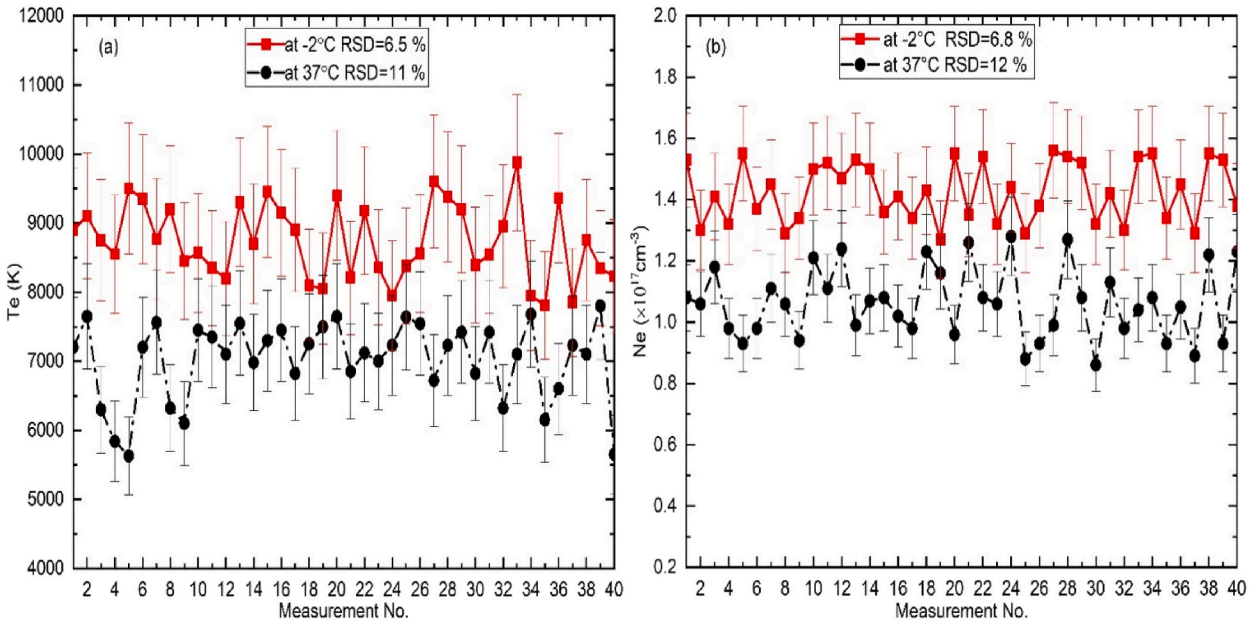

Fig. 11. (a, b): Measurement-to-measurement variation of T_e and N_e. The experimental conditions were: laser energy 150 mJ, DGDs 2 μs (for T = −2 °C), and 1 μs (for T = 37 °C).

Declaration of competing interest

The authors declare the following financial interests/personal relationships which may be considered as potential competing interests: SAMI UL HAQ reports administrative support, equipment, drugs, or supplies, and statistical analysis were provided by National Institute of Lasers and Optronics College, Pakistan Institute of Engineering and Applied Sciences, Nilore, Islamabad, 45,650, Pakistan. If there are other authors, they declare that they have no known competing financial interests or personal relationships that could have appeared to influence the work reported in this paper.

Acknowledgment

Acknowledgments.

M. Rashad Khan is gratified to the Pakistan Higher Education Commission (HEC) for financial support under the FDP scholarship and the Universiti Teknologi Malaysia (UTM) Johor Bahru for providing lab facilities to complete my experimental work.

References

[1] J.S. Kim, I.J. Kwon, M.G. Kim, J.Y. Chang, Won-bo shim, Food Control 79 (2017) 80–86.
[2] Che ManYaakob, Abdul Rohman, Tengku Mansor, Tengku Salwani, J. Am. Oil Chem. Soc. 88 (2011) 187–192.
[3] A.A. Aida, Y.B. Che Man, A.R. Raha, R. Son, J. Sci. Food Agric. 87 (2007) 569–572.
[4] O. Abbas, J.A. Fernández Pierna, R. Codony, C. von Holst, V. Baeten, J. Mol. Struct. 924–926 294–300 (2009).
[5] S.B. Smith, D.R. Smith, Encyclopedia of Food and Health, 608, UK Elsevier Ltd. F, Oxford, 2015, p. 604.
[6] Q. Abbas, M.A. Israr, S.U. Haq, Ali Nadeem, Optik 236 (2021) 166531.
[7] Y. Zhangcheng, Y. Liu, S. Saleem, Q. Zhang, Y. Chen, Y. Qu, X. Lu, J. Laser Appl. 32 (2020) 032020.
[8] X. Lu, Y. Liu, Q. Zhang, L. Li, Laser Phys. Lett. 17 (2020) 015701.
[9] Maria Markiewicz-Keszycka, Xavier Cama-Moncunill, Maria P. Casado-Gavalda, Yash Dixit, Raquel Cama-Moncunill, Patrick J. Cullen, Carl Sullivan, Trends Food Sci. Technol. 65 (2017) 80–93.
[10] D.A. Cremers, L.J. Radzeimski, Handbook of Laser-Induced Breakdown Spectroscopy, Wiley, New York, 2013.
[11] A.W. Miziolek, V. Palleschi, I. Schechter, Laser-Induced Breakdown Spectroscopy, Cambridge University Press, 2006.
[12] J.D. Winefordner, I.B. Gornushkin, T. Correll, E. Gibb, B.W. Smith, N. Omenetto, J. Anal. Atomic Spectrom. 19 (2004) 1061–1083.
[13] S.C. Jantzi, V. Motto-Ros, F. Trichard, Y. Markushin, N. Melikechi, A. De Giacomo, Spectrochim. Acta Part B At. Spectrosc. 15 (2016) 52–63.
[14] P. Yaroshchyk, R.J.S. Morrison, D. Body, B.L. Chadwick, Spectrochim. Acta Part B At. Spectrosc. 60 (2005) 986–999.
[15] K. Skočovská, J. Novotný, D. Prochazka, P. Pořízka, K. Novotný, J. Kaiser, Rev. Sci. Instrum. 87 (2016), 043116.
[16] A. Kumar, F.Y. Yueh, T. Miller, J.P. Singh, Appl. Opt. 42 (2003) 6040–6046.
[17] S.L. Zhong, Y. Lu, W.J. Kong, K. Cheng, R. Zheng, Frontiers of Physics 11 (2016) 1–9.
[18] A.N. Williams, S. Phongikaroon, Appl. Spectrosc. 70 (2016) 1700–1708.
[19] Y. Godwal, G. Kaigala, V. Hoang, S.L. Lui, C. Backhouse, Y. Tsui, R. Fedosejevs, Opt Express 16 (2008) 12435–12445.
[20] C. Janzen, R. Fleige, R. Noll, H. Schwenke, W. Lahmann, J. Knoth, P. Beaven, E. Jantzen, A. Oest P. Koke, Spectrochim. Acta Part B At. Spectrosc. 60 (2005) 993–1001.
[21] S. Groh, P. Diwakar, C. Garcia, A. Murtazin, D. Hahn, K. Niemax, Anal. Chem. 82 (2010) 2568–2573.
[22] H. Sobral, R. Sanginés, A. Trujillo-Vázquez, Spectrochim. Acta Part B At. Spectrosc. 78 (2012) 62–66.
[23] F.O. Borges, J.U. Ospina, G.H. Cavalcanti, E.E. Farias, A.A. Rocha, P.I.L.B. Ferreira, G.C. Gomes, A. Mello, J. Anal. Atomic Spectrom. 33 (2018) 629–641.
[24] X. Wang, Y. Wei, Q. Lin, J. Zhang, Y. Duan, Anal. Chem. 87 (2015) 5577–5583.
[25] N. Syaida, R.K. Raja Ibrahim, M. Duralim, H.H. Jameela, M.A. Mahdi, Appl. Spectrosc. 74 (2020) 1452–1462.
[26] Atomic Spectra Database NIST (https://www.nist.gov/pml/atomic-spectra-database).
[27] R.E. Russo, Laser ablation, Appl. Spectrosc. 49 (1995) 14A–28A.
[28] L. Chen, H. Deng, Z. Xiong, J. Guo, Q. Liu, G. Li, L. Shang, Photonics 8 (2021) 536–549.
[29] 10 Chp, J.P. Singh, S.N. Thakur, Laser-induced Breakdown Spectroscopy, Elsevier Science BV, 2007.
[30] K. Keerthi, S.D. George, S.D. Kulkarni, S. Chidangil, V.K. Unnikrishnan, Opt Laser. Technol. 147 (2022) 107622.
[31] J.B. Sirven, P. Mauchien, B. Sallé, Spectrochim. Acta, Part B 63 (2008) 1077–1084.
[32] C. Li, L. Guo, X. He, Z. Hao, X. Li, M. Shen, X. Zeng, Y. Lu, J. Anal. At. Spectrom. 29 (2004) 638–643.
[33] J.A. Aguilera, C. Aragón, Spectrochim. Acta Part B At. Spectrosc. 59 (2004) 1861–1876.
[34] J.A. Aguilera, C. Aragon, Spectrochim. Acta Part B At. Spectrosc. 62 (2007) 378–385.
[35] El Sherbini, A. Hegazy, H. El Sherbini, Spectrochim. Acta Part B At. Spectrosc. 61 (2006) 532–539.
[36] H.R. Griem, Spectral Line Broadening by Plasmas, Academic Press, New York, 1974.